Journal of ELECTRONIC MATERIALS, Vol. 46, No. 2, 2017
DOI: 10.1007/s11664-016-5060-x

Substrate Effects on Growth of MoS_2 Film by Laser Physical Vapor Deposition on Sapphire, Si and Graphene (on Cu)

K. JAGANNADHAM ,[1,3] J. CUI,[2] and Y. ZHU[2]

1.—Department of Materials Science and Engineering, North Carolina State University, Raleigh, NC 27695, USA. 2.—Department of Mechanical and Aerospace Engineering, North Carolina State University, Raleigh, NC 27695, USA. 3.—e-mail: jag_kasichainula@ncsu.edu

Molybdenum disulfide (MoS_2) films were deposited on sapphire (0001), Si (001) and graphene on Cu by laser physical vapor deposition at 600°C for different time periods to achieve control of thickness. MoS_2 film was found to grow on all the substrates in the (0002) orientation. Films are found to be S-deficient and a free Mo peak was observed in the x-ray diffraction. Raman spectroscopy showed the characteristic peaks of MoS_2 film with decreasing separation between the A_{1g} and E^1_{2g} peaks for a shorter time of deposition or smaller thickness of the film. MoS_2 films on sapphire substrate showed additional peaks due to MoO_3 and Mo_4O_{11} phases. Films on Si substrate and graphene on Cu contained only the characteristic peaks. MoS_2 films on graphene suppressed the graphene peak as a result of large fluorescence background in the Raman spectrum. Interfacial effects and the presence of an oxygen impurity are considered responsible for the large fluorescence background in the Raman spectrum. X-ray photoelectron spectroscopy indicated substrate interaction with the films on sapphire and Si. Coverage of the film on the substrates is uniform with uniform distribution of the Mo and S as evidenced from the x-ray maps. Atomic force microscopy image revealed the surface of the film on sapphire to be very smooth. Electrical conductance measurements showed the MoS_2 film on sapphire is semiconducting but with much lower activation energy compared to the bandgap. The presence of excess Mo in the film is considered responsible for the lower activation energy.

Key words: Molybdenum disulfide, graphene, laser deposition

INTRODUCTION

Molybdenum disulfide (MoS_2) thin films have been investigated for several applications including electronic,[1] solar,[2] and optoelectronic devices,[3] photo catalyst in hydrogen generation,[4,5] battery electrodes[6] and lubricant films.[7] MoS_2 exhibits a direct band gap of 1.8 eV in films of one monolayer,[8] and and indirect bandgap of 1.2 eV in its bulk form.[9] The presence of the band gap is considered a specific advantage over graphene films as it is a requirement for device structure.[10]

Many studies of MoS_2 devices and characterization of properties are carried out on films prepared by mechanical exfoliation.[11,12] Synthesis of MoS_2 films by chemical vapor deposition (CVD)[13,14] and laser physical vapor deposition (LPVD)[15] is attempted for large-scale adoption of MoS_2 in many applications. Integration of MoS_2 films with graphene to form the heterostructure is considered an opportunity[16–18] to tailor the electronic transport in graphene. The interface between graphene and MoS_2 films is an important region that is responsible for altering the electron transport.[19]

Characterization of the defect structure in the films revealed[20,21] many categories of defects including vacancies resulting from sulfur deficiency and presence of impurities such as oxygen. Dislocations and grain boundaries[22] are observed in polycrystalline films. The thickness and perfection of the

(Received June 14, 2016; accepted October 13, 2016; published online October 28, 2016)

MoS_2 films are important parameters that control the bandgap and the carrier mobility.[21] It has been found that in CVD,[22] that cleaner substrates were important in the growth of defect-free crystals. When the substrates were dirty, defect-free triangular crystals were replaced with defective regions.[22] The thickness of the crystals was dependent on the position of the substrate with respect to the source; it was larger when the substrate was closer and negligible when substrate was farther. Multiple nucleation sites of the films during growth were responsible for formation of both tilt and twist boundaries when the crystals coalesced, although only tilt boundaries were found to be responsible for altering the conductivity.[22] Also, surface defects consisting of charged impurities, short range disorder such as interfacial bonding or roughness and sensitivity to the ambient environment were observed, giving rise to a transition from hopping conductivity[21] to bulk conducting behavior at a larger thickness. For smaller thickness up to 2 or 3 monolayers, sulfur vacancies are found responsible for carrier scattering, resulting in hopping conductivity. Sulfur vacancies are generally predominant defects because of the low energy of formation and higher vapor pressure of sulfur. Sulfur deficiency and Mo excess naturally leads to *n*-type MoS_2 conductivity.[20] Antisite defects with Mo occupying S positions (Mo_S) are found to be dominant defects in films grown by physical vapor deposition.[20]

In the present work, we have used LPVD to deposit films of MoS_2 on different substrates including (0001) sapphire, (001) Si and graphene on copper. The films were characterized by different techniques to determine the substrate effects on the film growth and properties. These results will be useful to deposit MoS_2 films for device applications provided additional techniques for incorporation of electrically active dopants and contacts are determined.

EXPERIMENTAL DETAILS

The polished sapphire and Si substrates used in the deposition of MoS_2 films were cleaned in acetone and isopropyl alcohol and dried with nitrogen. The Si substrate was further etched in 49% HF for 1 min and rinsed with deionized water and dried. The graphene on copper substrates were prepared by microwave plasma CVD of graphene on Cu. Polycrystalline Cu foils with thicknesses close to 100 μm were polished to smoothness using 600-, 800- and 2400-grade SiC polishing paper supplied by Struers Inc. The Cu foils were further etched with a mixture of 50% H_2SO_4 and 50% HNO_3 in distilled water for 3 min to remove any abrasive particles present on the surface.

Deposition of Graphene on Cu Foils by Microwave Plasma Deposition (MWCVD)

Cu foils of size 0.5 cm by 0.5 cm and thickness of 100 μm were loaded on to the substrate holder in an 8-inch diameter stainless steel MWCVD chamber equipped with an ASTEX Inc. 1.5-KW power supply. The chamber was evacuated by means of a mechanical pump and gas pressure controlled by an MKS Instruments Inc. exhaust valve controller. The H_2 and CH_4 gas flow into the chamber is controlled by MKS Instruments Inc., flow meters. In addition, nitrogen and argon gas inlets were provided by two needle valves. The graphite substrate holder was heated by means of a tungsten filament heater that could go up to 600°C. The tuners were adjusted to stabilize the microwave plasma above the substrate. The presence of the plasma was observed through a quartz window. The temperature of the substrate holder was measured with a thermocouple situated below the graphite substrate holder.

The chamber was evacuated by means of a mechanical pump to 1 mTorr (0.133 Pa) pressure and purged with H_2 gas. The substrate was heated to 600°C in the presence of H_2 gas at a pressure of 30 Torr (4 kPa) and flow rate of 25 sccm with a direct current of 20 amps and voltage of 20 V. The microwave power supply was turned on and increased to 850 W slowly with the plasma generated above the sample. The sample was treated in H_2 plasma for 20 min at 900°C. At this point, the methane valve was opened and the flow of methane was controlled at 10 sccm while the H_2 gas supply was turned off. The sample was treated in methane plasma for 20 min. The microwave power and the substrate heater were turned off and the sample was allowed to cool. Simultaneously, H_2 gas flow was started while the sample was cooled to room temperature. H_2 flow was stopped when the temperature was below 200°C. Several samples with graphene film on Cu foil were prepared for further deposition of MoS_2 on graphene.

Deposition of MoS_2 by Laser Physical Vapor Deposition (LPVD)

MoS_2 films were deposited on sapphire (0001), Si (001) and graphene on Cu substrates. In each deposition that was carried out for a specified period of time, the three substrates were held side by side on the substrate holder so that the depositions conditions remained the same. All the three substrates, with size close to 0.5 cm × 0.5 cm, were held on the substrate holder (5 cm × 8 cm in area) by colloidal silver paste to maintain uniform temperature during LPVD. The MoS_2 target was 2.5 cm in diameter and 0.8 cm in thickness. The target was cleaned with a sharp blade before each deposition so that the previously laser-ablated region was removed and fresh MoS_2 was exposed. An Nd-YAG laser in the fourth harmonic (λ = 266 nm), pulse energy of 210 mJ, a duration 6 ns, a beam diameter 8 mm and a repetition rate of 10 Hz were used for laser ablation. The substrate holder was heated by means of a resistance heater to 600°C. The target to substrate distance was maintained at 4 cm. The

chamber was evacuated by means of a turbo pump backed by a mechanical pump to achieve a pre-deposition vacuum of 5×10^{-7} Torr (0.067 mpa) upon baking at 150°C. The deposition was carried out for different periods of time; 15 s, 20 s, 45 s, 1 min and 15 min to examine if the thickness of the deposited film was reduced successfully on each substrate for shorter deposition time. The samples were cooled at a rate of 5° per min initially until the temperature reached 500°C and then at 10° per min so that thermal stresses responsible for nucleation of defects and film cracking were not generated.

Characterization of the MoS_2 and Graphene Films

MoS_2 and graphene films were characterized by scanning electron microscopy (SEM) for surface morphology and microstructure, energy dispersive spectrometry (EDS) for composition, atomic force microscopy (AFM) for surface smoothness, Raman spectroscopy for the lattice perfection, x-ray photoelectron spectroscopy (XPS) to determine the substrate interaction and x-ray diffraction to identify the phases when the deposition time was large enough to give sufficient counts of the diffraction peaks. Graphene films did not exhibit peaks with enough counts and, hence, were not characterized by x-ray diffraction. Electrical conductance of the MoS_2 films on sapphire substrate was measured by the four probe technique. MoS_2 films on Si and graphene on Cu were not characterized for electrical conductance as the substrates were conducting.

EXPERIMENTAL RESULTS AND DISCUSSION

X-ray Diffraction of MoS_2 Films

Results of x-ray diffraction were obtained using a Rigaku instrument in the $\theta - 2\theta$ configuration. Peak profiles are shown in Fig. 1a for the MoS_2 films deposited on sapphire (0001) substrates at 600°C. The MoS_2 (0002) peak at 14. 4° was not observed in the films deposited for 45 s; however, a broad peak was present for the film deposited for 1 min, and a much stronger peak for the film deposited for 15 min. In addition, a broad peak was observed near $2\theta = 39°$ in the film deposited for 1 min that could be associated with S-deficient MoS_2. A peak associated with Mo (110) at $2\theta = 40.5°$ was observed in the film deposited for 15 min which indicates that the film is deficient in S.

The diffraction peak profiles are shown in Fig. 1b for MoS_2 films deposited on Si (001) substrates at 600°C. An MoS_2 (0002) peak was observed in the film deposited for 15 min along with Mo (220) peak indicating that S deficiency is present. However, the (0002) MoS_2 peak was not observed in the films deposited for 1 min. The diffraction peak profiles are shown in Fig. 1c for MoS_2 films deposited on polycrystalline Cu substrates at 600°C. The results show that a strong MoS_2 peak is absent even after 15 min deposition but a weak Mo (110) peak is present. A very weak MoS_2 (0002) peak is present at $2\theta = 14.4°$.

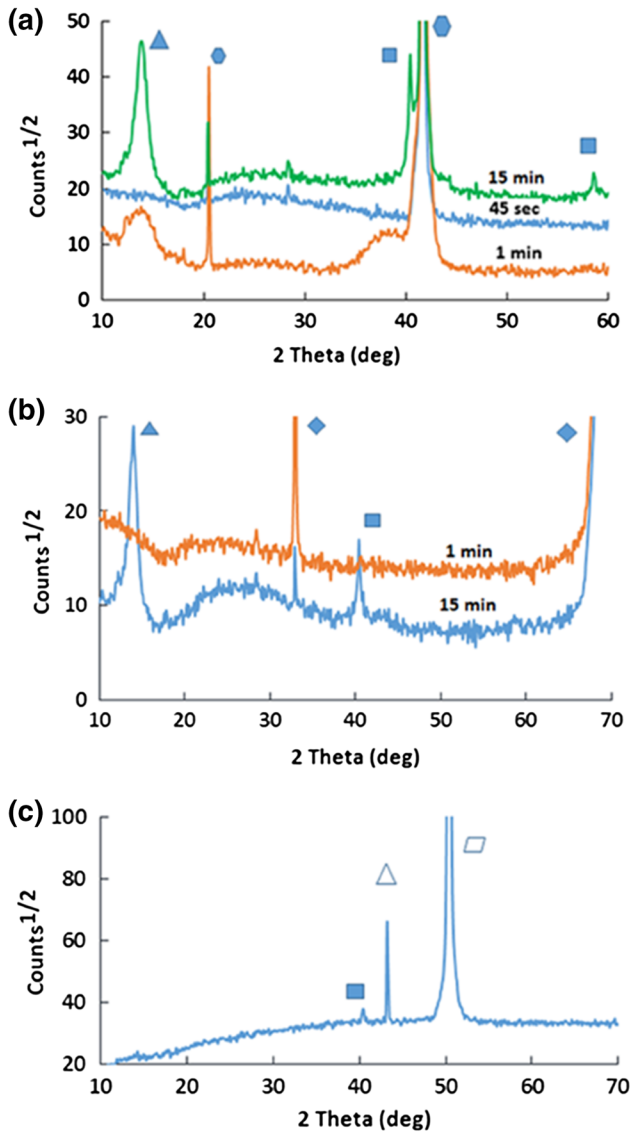

Fig. 1. (a) X-ray diffraction peak profile from the MoS_2 film deposited on sapphire (0001) substrate for 45 s (3 layers), 1 min (4 layers) and 15 min (bulk) at 600°C. The filled triangle represents MoS_2 (0002), hexagons represent sapphire (0002) and (0004) and squares represent Mo (110) and (200). The broad peak near 39° was from MoS_2. The number of atomic layers was determined from the Raman spectrum. (b) x-ray diffraction peak profile from MoS_2 film deposited on Si (001) substrate for 1 min (5 to 6 layers) and 15 min (bulk) at 600°C. The filled triangle represents the MoS_2 (0002) peak, diamond represents the Si (002) and (004) peaks, and square represents Mo (110) peak. Films deposited for 1 min did not show any MoS_2 peak. The number of atomic layers was determined from the Raman spectrum. (c). x-ray diffraction peak profile from MoS_2 film deposited on Cu substrate for 15 min at 600°C. The filled square represents Mo (110), the open triangle represents Cu (111) and the open parallelogram represents Cu (220) peak. A very weak peak from MoS_2 (0002) is present at 14.4°.

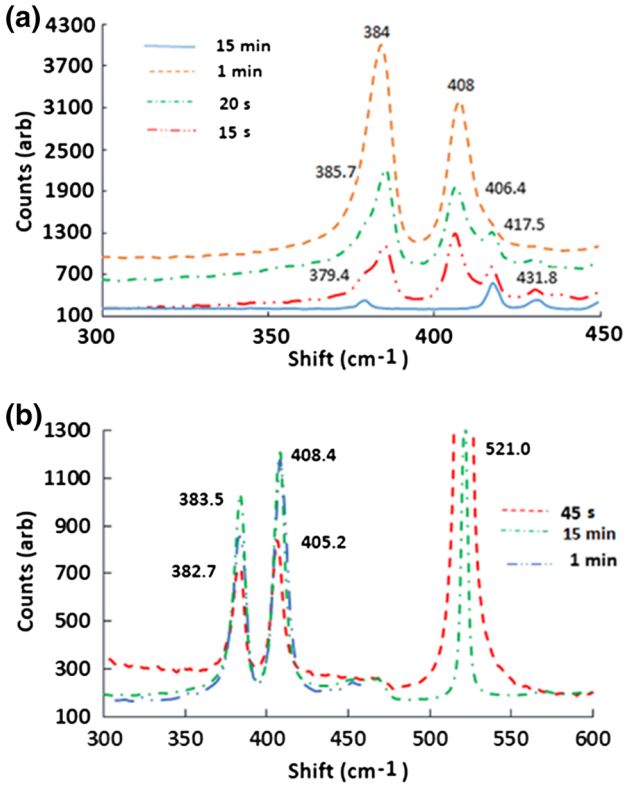

Fig. 2. (a) Raman spectrum from MoS_2 film on sapphire substrate using 442-nm laser excitation wave length. The largest separation between the A_{1g} and E^1_{2g} peaks of MoS_2 was 23.8 cm^{-1} for films deposited for 1 min and the smallest separation was 20.6 cm^{-1} for films deposited for 20 s and below. the peak close to 380 cm^{-1} is from MoO_3, and the peaks at 431 cm^{-1} and 451 cm^{-1} are from Mo_4O_{11} phases. The peak at 417.5 cm^{-1} is the A_{1g} peak from sapphire. The results for different films are shifted vertically. (b) Raman spectrum from MoS_2 film on Si substrate using a 442-nm laser excitation wave length. The largest separation between A_{1g} and E^1_{2g} peaks is 24.9 cm^{-1} in the film deposited for 15 min and the shortest separation was 22.5 cm^{-1} in film deposited for 45 s. Also, no other oxide peaks were observed.

Growth of films on sapphire and Si indicates that preferred (0002) orientation is present. However, the thickness of film grown for 1 min on Si was not enough to give an x-ray peak, whereas that on sapphire gave a broad peak. In addition, the presence of an Mo peak signifies that the films are deficient in S. Thicker lubricating films deposited by LPVD are known to be deficient in S.[23] Laser ablation is responsible for breaking the Mo-S bond and S is lost preferentially, in particular, in the presence of a small concentration of O in the chamber at 6.67 $\times$ 10^{-8} kPa. Excess S in the target could overcome the deficiency. Interaction of the Cu substrate with the film was also responsible for loss of S from the film. Film deposited for 15 min on Cu showed only a very weak peak of MoS_2 (0002) that was not easily identified. Thus, S reacts with Cu, leaving free Mo in the film,[24] as shown in Fig. 1c.

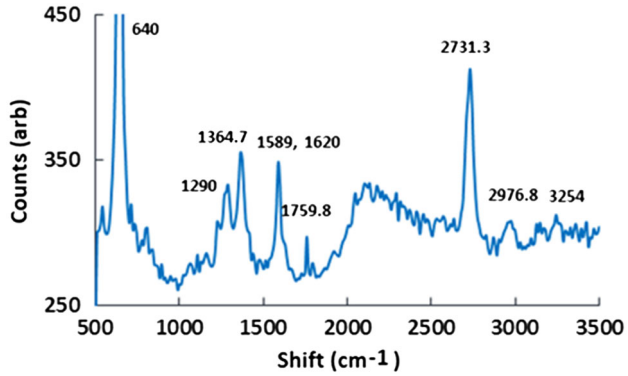

Fig. 3. Raman spectrum from graphene film on Cu foil using a 442-nm laser excitation wave length. The Raman primary peak at 640 cm^{-1} is from CuO and the peak at 1290 cm^{-1} is the second order peak. The D peak is observed at 1364.7 cm^{-1}, the G peak at 1589 cm^{-1} and the peak at 1620 cm^{-1} is from glassy carbon phase. The 2D peak at 2731.3 cm^{-1} is from graphene. The peak at 2976.8 cm^{-1} is from C-H bond stretching and peak at 3254 cm^{-1} and higher wave numbers are a result of sum of D, G and 2D peaks.

Raman Spectroscopy

Raman spectra of the films were collected using a Lab RAM Horiba Scientific instrument with a microscope at 100$\times$ and laser excitation wave length of 442 nm to avoid a fluorescence background. In addition to E^1_{2g} and A_{1g} peaks from MoS_2, other peaks that arose from oxides of Mo and sapphire were observed, as shown in Fig. 2a. The A_{1g} peak from the MoS_2 film deposited for 15 min appeared at 417.5 cm^{-1} which is close to the A_{1g} peak of sapphire. The peak was weak. Similarly, the E^1_{2g} peak in the film deposited for 15 min appeared at 379.4 cm^{-1} and it is close to MoO_3 peak. Thus, the peaks from MoS_2 in the film deposited for 15 min were weak and could not be separated from the peaks from MoO_3 at 379.4 cm^{-1} and sapphire at 417.5 cm^{-1}. The results could also be due to presence of S deficiency or free Mo and interaction of O in sapphire with MoS_2. However, the E^1_{2g} and the A_{1g} peaks were clearly identified in other films and the separation between the peaks decreased for shorter deposition time up to 15 s.

The E^1_{2g} peak due to in-plane vibrations[25] and the A_{1g} peak due to out of plane vibrations[25] were shifted farthest in films deposited for 15 min, and the separation continuously decreased as the time for deposition was reduced to 15 s. The formation of MoS_2 film after 15 s on sapphire was clearly verified from the Raman spectrum. Thus, although x-ray diffraction is unable to detect the formation of MoS_2 layers, the Raman spectrum provided proof of the formation. The peaks beyond 417.5 cm^{-1} arose from the MoO_3 and Mo_4O_{11} phases.[26,27] The formation of oxides of Mo in the film appears to be a result of reaction with the sapphire substrate as those peaks are not observed in the films deposited on Si substrate, although the two substrates were placed next to each other during deposition. The presence

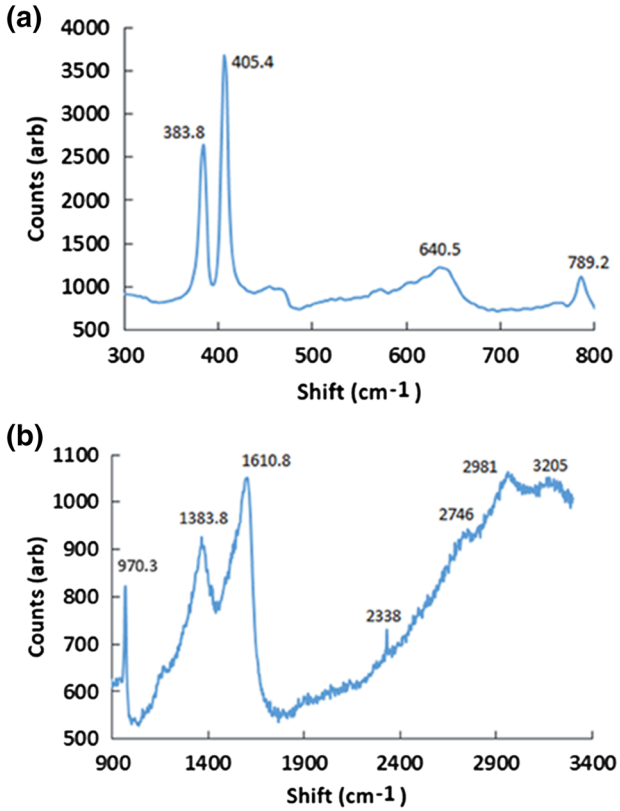

Fig. 4. (a) Raman spectrum from MoS_2 film deposited for 45 s on graphene film on Cu foil using a 442-nm laser excitation wave length. The MoS_2 range is shown. (b) Raman spectrum from MoS_2 film deposited for 45 s on graphene film on Cu foil using a 442-nm laser excitation wave length. The graphene range is shown.

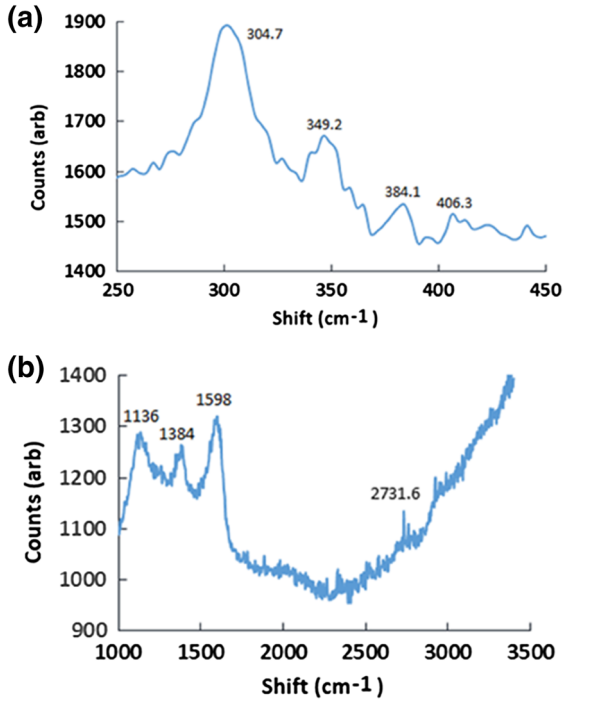

Fig. 5. (a) Raman spectrum from MoS_2 film deposited for 20 s on graphene film on Cu foil using a 442-nm laser excitation wave length. The MoS_2 range is shown. The peak positions are not determined exactly as the peaks are broad. (b) Raman spectrum from MoS_2 film deposited for 20 s on graphene film on Cu foil using a 442-nm laser excitation wave length. The graphene range is shown.

of free Mo will be responsible for the film to be semiconducting but with lower activation energy.

The Raman spectrum of films deposited on Si (001) is presented in Fig. 2b. In addition to the first-order Raman peak at 521 cm^{-1} from Si, the E^1_{2g} and A_{1g} peaks from MoS_2 are present. Peaks from MoO_3 or Mo_4O_{11} are absent. The largest separation between the two peaks was 24.9 cm^{-1} for the MoS_2 film deposited for 15 min and the smallest separation was 22.5 cm^{-1} for the film deposited for 45 s. Raman spectrum from films deposited for 15 s and 20 s did not exhibit clear peaks from MoS_2. Therefore, substrate interaction with Mo forming a very thin layer of $MoSi_2$ was possible.

The Raman spectrum of graphene film deposited on Cu substrate is shown in Fig. 3. The peak from CuO is observed at 640 cm^{-1}. The peak at 1290 cm^{-1} is considered to be the second-order CuO peak. The D peak and G peak from the graphene film are observed at 1364.7 cm^{-1} and 1589 cm^{-1}, respectively.[28–30] The peak at 1620 cm^{-1} is from the glassy carbon phase[31,32] and the 2D peak at 2731.3 cm^{-1} is from graphene. The 2D peak is symmetric and much stronger than the G peak, indicating that the graphene film is either a single or bilayer of carbon atoms. However, the polycrystalline nature of the film is responsible for grain boundaries where disorder is present. This disorder is responsible for the presence of the D peak in the spectrum. A higher order peak at 2976.8 cm^{-1} arises from C-H bonds in the film and the second order peaks are present at higher values of wave number.[28–32] Thus, the graphene films are highly crystalline.

Raman spectra of the MoS_2 films deposited for 45 s and 20 s on graphene film grown on Cu are shown in Figs. 4 and 5, respectively. The results are shown for two different ranges; the MoS_2 and the graphene range. The Raman spectrum shown in Fig. 4a indicates that the E^1_{2g} and A_{1g} peaks are strong with a separation of 21.6 cm^{-1}. The peak at 640.5 cm^{-1} is from CuO. The peak at 789.2 cm^{-1} has not been identified previously but it is the second-order peak from MoS_2, $2E^1_{2g}$.[33,34] The Raman spectrum from the same sample in the graphene range or above 900 cm^{-1}, presented in Fig. 4b, contains the D and G peaks at 1383.8 cm^{-1} and 1610.8 cm^{-1}, respectively. The broad peak at 1610.8 cm^{-1} is a superposition of the G peak at 1588 cm^{-1} and the glassy carbon peak near 1610 cm^{-1}. The background from fluorescence beyond 1900 cm^{-1} has increased significantly due to MoS_2 film on graphene. The Raman peak labeled 2D associated with graphene, observed at 2731 cm^{-1} in Fig. 3, was shifted to 2746 cm^{-1}. Similarly, the peaks at 2976.8 cm^{-1} and above were shifted to 2981 cm^{-1} and higher values, respectively.

Table I. Frequency difference ($\Delta\nu$) in Raman shift (cm^{-1}) between A_{1g} and E^1_{2g} peaks of MoS_2 film deposited on the three substrates and the thickness of the films in number of layers (n)

	Sapphire		Silicon		Graphene (on Cu)	
Time of deposition (min)	$\Delta\nu$	n	$\Delta\nu$	n	$\Delta\nu$	n
0.25	20.6	1 to 2	–	–	–	–
0.33	20.6	1 to 2	–	–	–	–
0.75	22.0	3	22.5	3 to 4	21.6	2 to 3
1.0	23.8	4	24.0	5 to 6	22.0	3
15.0	38.1	Bulk	25.0	Bulk	-	–

The number of layers is determined based on results from Ref. 25. The separation between layers is between 0.6 nm and 0.7 nm.[25] The three substrates were placed next to each other on the substrate holder during deposition for each specified time. The films deposited on Si and graphene for time below 45 s showed broad peaks and the peak positions could not be determined exactly.

Thus, the presence of MoS_2 film has shifted the positions of all the peaks in the graphene range to higher values. The peak at 970.3 cm^{-1} has not been identified previously with a laser excitation wave length of 442 nm used in the present investigation. However, a peak at 980 cm^{-1} has been identified as a T-peak and arises from C-C bonds in the carbon films but is only observed when the excitation wave length is in the ultra violet (UV) range.[31] The peak at 970.3 cm^{-1} is observed only in the presence of MoS_2 film on graphene as it is absent in the spectrum associated with graphene on Cu, shown in Fig. 3.

The Raman spectrum of the MoS_2 film deposited for 20 s on graphene on Cu is presented in Fig. 5a for the MoS_2 range. The E^1_{2g} and A_{1g} peaks are very week and broad, indicating that a good crystalline film has not formed. In addition, the peaks from CuO at 304.7 cm^{-1}, 349.2 cm^{-1} are present. The peaks at 384.1 cm^{-1} and 406.3 cm^{-1} are weak and arise from MoS_2 but the positions are difficult to determine as they are broad. The film is not expected to be highly crystalline and may not be a continuous monolayer. The Raman spectrum of the film covering the graphene range or above 1000 cm^{-1} is presented in Fig. 5b. The D and G peaks are present at 1384 cm^{-1} and 1598 cm^{-1}. The 2D peak from graphene and other peaks are very weak in the presence of a large background from fluorescence. The peak at 1136 cm^{-1} was not identified previously but it is the second order peak from CuO. Although the peak positions are not significantly shifted by the presence of MoS_2 film on the top, the fluorescence background is responsible for a weak 2D peak from graphene at 2731.6 cm^{-1}.

Results of Raman spectroscopy on films on different substrates illustrate that stoichiometric MoS_2 is present. However, the presence of other phases is also identified. In addition, Raman spectra could not be obtained from films deposited on Si below 45 s. Thus, the sticking coefficient of the MoS_2 films is low and substrate interaction with the film is possible. Therefore, XPS characterization was further carried out. The thickness of the films or the number of atomic layers (n) on different substrates was determined based on the correlation between 'n' and the frequency difference $\Delta\nu$ between the A_{1g} and E^1_{2g} peaks[25] and the results are presented in Table I. It should be noted that the results are influenced by the substrate interaction with the film. Films with one or two atomic layers are not detected on Si substrate.

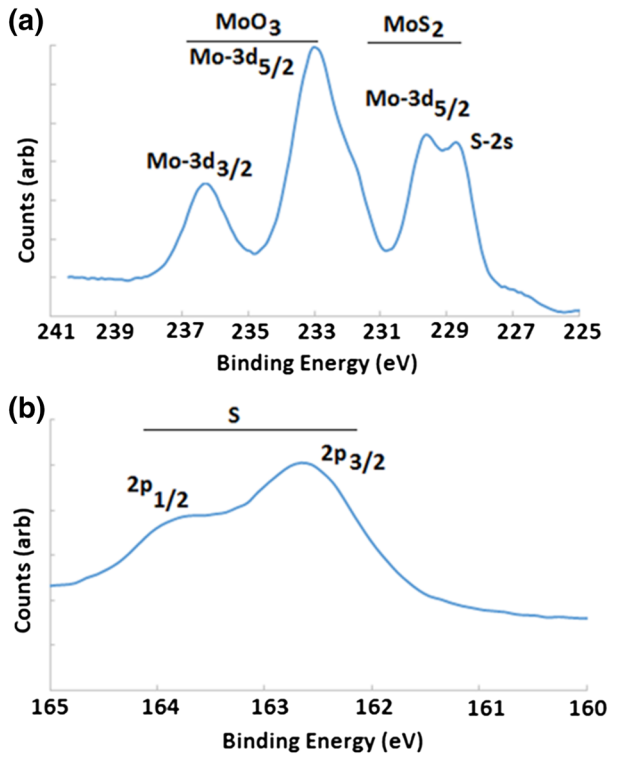

Fig. 6. XPS results of MoS_2 film on sapphire for (a) Mo 3*d* and S 2*s* peaks, (b) S 2*p* peaks. The MoO_3 peaks are very strong, indicating sapphire interaction with the film.

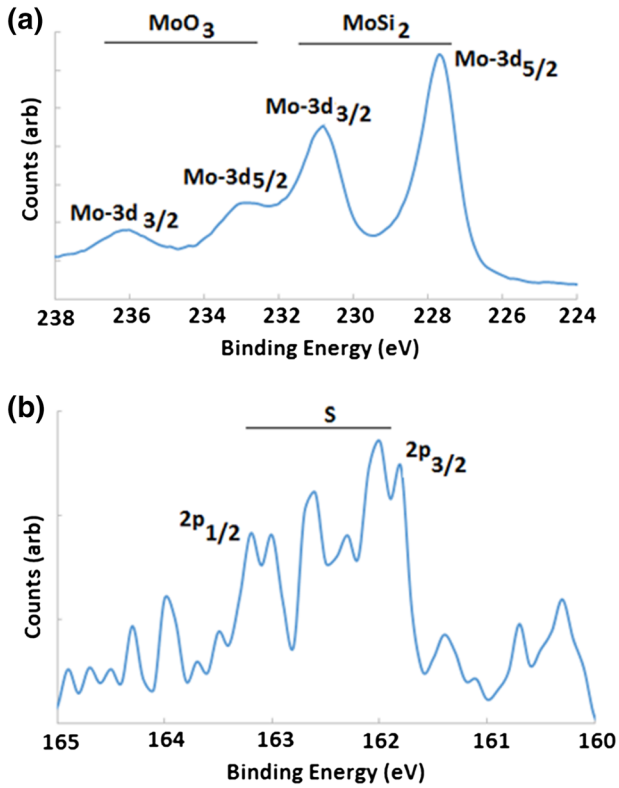

Fig. 7. XPS results of MoS2 film on Si for (a) Mo 3*d* and S 2*s* peaks, (b) S 2*p* peaks. The S 2*s* peak is very weak. The signal-to-noise ratio for the S 2*p* peaks is also not high, indicating that the films are S-deficient. Mo 3*d* peaks appear to be due to $MoSi_2$ formation. MoO_3 peaks are not very strong, indicating that surface oxidation is responsible for the interaction with MoS_2 film.

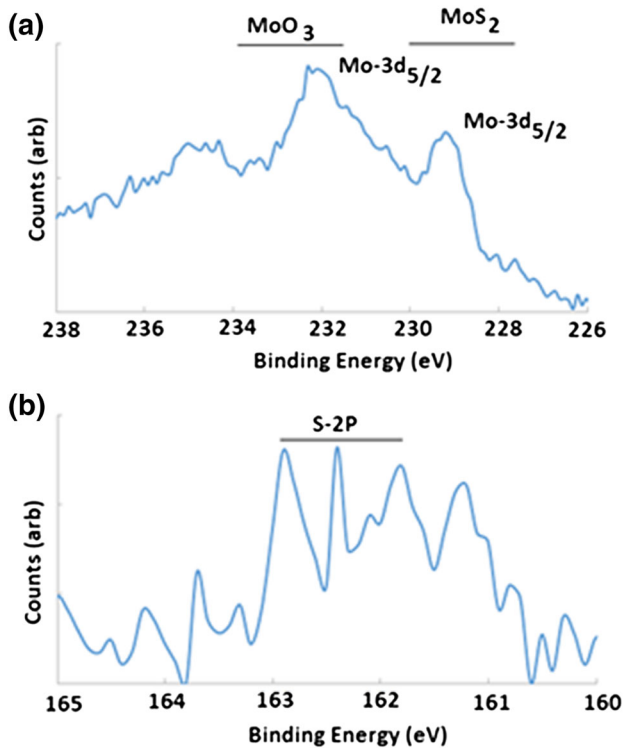

Fig. 8. XPS results of MoS_2 film on graphene on Cu for (a) Mo 3*d* peaks, (b) S 2*p* peaks. The S 2*s* peak is very weak. The signal-to-noise for the S 2*p* peaks is also not high, indicating that the films are S-deficient. Interaction of C with MoS_2 to form MoC is not found as C is incorporated in MoO_3.

X-ray Photoelectron Spectroscopy (XPS)

XPS was performed using a SPECS Flexmod instrument with Mg kα excitation. The analyzer was a PHOIBOS 150 with a takeoff angle normal to the sample surface. Results of XPS for MoS_2 film deposited for 1 min on sapphire, Si and graphene on Cu are shown in Figs. 6–8, respectively. XPS provides values of binding energy of electronic states of elements in phases present in the film in the top 3 to 4 monolayers. Although Raman spectroscopy showed strong peaks associated with MoS_2 in films deposited for 1 min, XPS showed differences in the surface layers. These results are useful to understand the substrate effects.

The results shown in Fig. 6 indicate the presence of strong Mo 3*d* peaks consistent with the MoO_3 phase[35] and MoS_2.[14,35] Interaction of sapphire with MoS_2 film and formation of MoO_3 is previously noted from Raman spectrum shown in Fig. 2a. Surface oxidation of MoS_2 is also expected to give rise to MoO_3 formation[36,37] in the surface layers. There is a S 2*s* peak that causes some interference with the Mo 3*d* 5/2 peak for MoS_2. The presence of Mo 3*d* peaks in $MoSi_2$ [37,38] and MoO_3 and absence of MoS_2 in Fig. 7a indicate that the film is S-deficient. The signal from S 2*p* peaks, shown in Fig. 7b, is also weak and noisy. Thus, Si interaction with Mo to form $MoSi_2$ is evident. Results of Raman spectroscopy, shown in Fig. 2b, indicate clearly that MoS_2 is present on Si in the film deposited for 1 min. However, films containing one to two atomic layers could not be obtained. Therefore, formation of $MoSi_2$ in the surface layers is a substrate effect. Absence of MoS_2 in the surface is due to S deficiency. Results presented in Fig. 8a show the Mo 3*d* peaks from MoS_2 and MoO_3 in the film deposited for 1 min on graphene on Cu. The S 2*s* and 2*p* peaks, shown in Fig. 8b, are also weak. Peaks associated with MoC[39] are difficult to assign because C is incorporated in MoO_3. Also, the peak positions depend on the charged state of Mo.[39,40] Thus, interaction of MoS_2 with graphene is not evident. The weak van der Walls bonding between graphene and MoS_2 is responsible for the absence of interaction between Mo and C.

Scanning Electron Microscopy (SEM) and Atomic Force Microscopy (AFM)

SEM imaging was carried out using an FEI Verios Inc., 460 L and Oxford Inc., high count EDS detector. The secondary electron image of MoS_2 film deposited on sapphire (0001) for 1 min is shown in Fig. 9a with the EDS spectrum in Fig. 9b. The

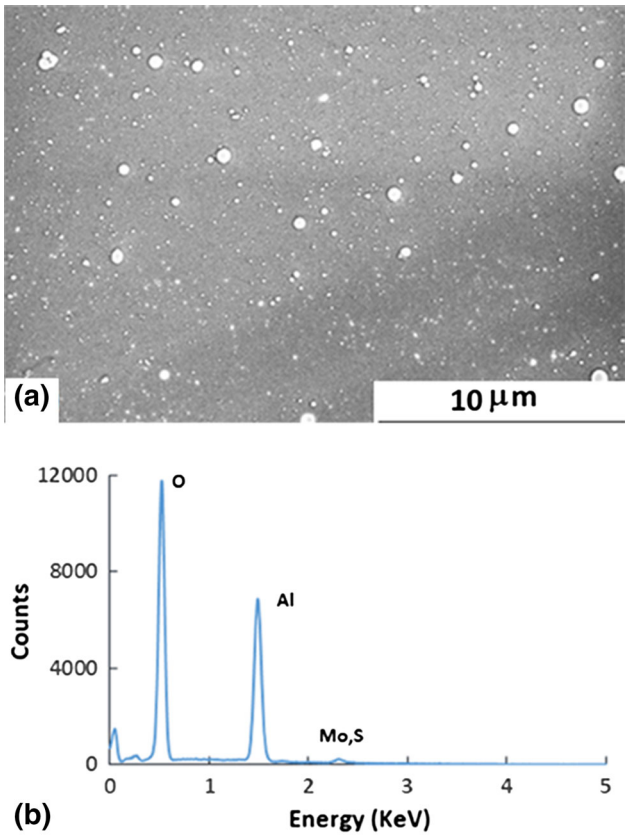

Fig. 9. (a) SEM image in secondary electron mode of MoS_2 film deposited on sapphire (0001) for 1 min. (b) EDS spectrum from MoS_2 film deposited on sapphire (0001) for 1 min. The EDS counts were collected for close to 15 s beyond which the O signal was saturated.

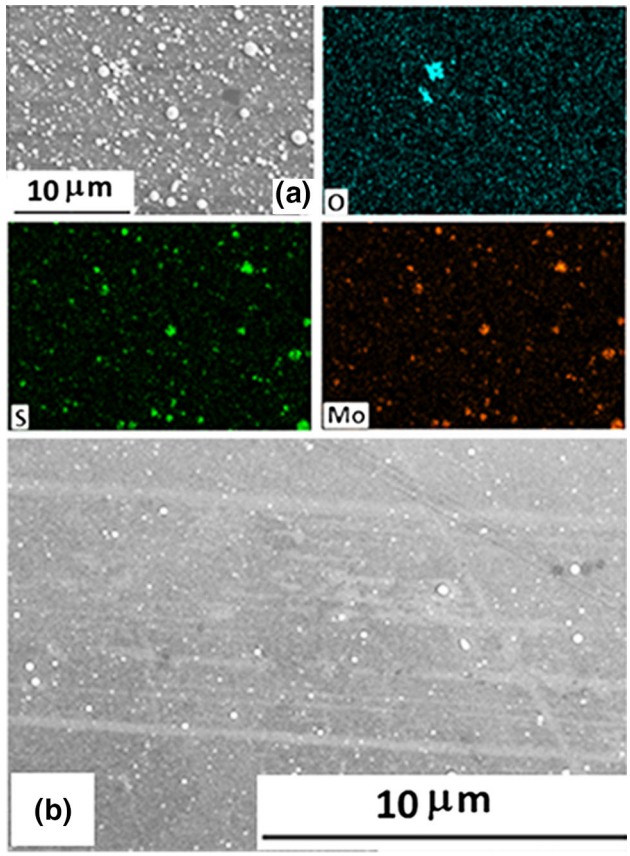

Fig. 10. (a) SEM image in secondary electron mode of MoS_2 film deposited on Si(001) for 45 s. (b) SEM image in the secondary electron mode of MoS_2 film deposited on Si(001) for 20 s.

circular-shaped particles are the laser-generated molten droplets from the target that solidified upon reaching the sapphire substrate. The EDS spectrum, presented in Fig. 9b, contains only the Al, O, Mo and S peaks to be present from the film. The EDS signal was collected for nearly 15 s so that the maximum in the counts for O was saturated. However, the counts from Mo and S signal were lower because the film is only a few monolayers. The Mo to S atomic ratio is found from the software of the instrument to be 0.8 to 1.2. Thus, the films are found to be S-deficient. The films on the substrate contain different phases, and peaks from all the elements are present in EDS. Thus, the estimates of nonstoichiometry from the instrument software may not be accurate in the presence of different phases. However, the films contain excess Mo or S vacancies that will be responsible for the film to be an *n*-type semiconductor with lower activation energy for electrical conductance.

SEM image of MoS_2 film deposited on Si for 45 s and 20 s is shown in Fig. 10a and b, respectively, along with the x-ray maps of elements Mo, S and O shown in Fig. 10a. The x-ray maps illustrate a uniform distribution of Mo and S. The strong O signal is only from particle contamination on the surface seen in the SEM image. Otherwise, the O signal from MoS_2 films is low. The films are found to be S-deficient from the EDS spectrum that is not shown. The signal from the Mo and S, shown in Fig. 10a, is not very strong compared to that from the Si substrate as a result of very few atomic layers of MoS_2. Results of the Raman spectrum from Fig. 2b and the SEM image of the film for 45 s indicate that good crystalline quality MoS_2 film was grown on Si (001). The MoS_2 film on Si deposited for 20 s is found to be nonuniform in thickness, as shown in Fig. 10b. Streaks of bright areas are separated by dark areas representative of MoS_2 in the image. Thus, a deposition time of at least 30 to 45 s is needed for continuous coverage on the Si substrate as the sticking coefficient of MoS_2 to Si is not high and $MoSi_2$ is found to form.

SEM images of graphene film deposited by microwave plasma CVD are presented in Fig. 11 in the backscattering and secondary electron modes. The regions with different shades in the backscattering image illustrate the variation of thickness of the graphene film. The secondary electron image on the right also contains regions where the film is thinner and seen as brighter regions. The graphene

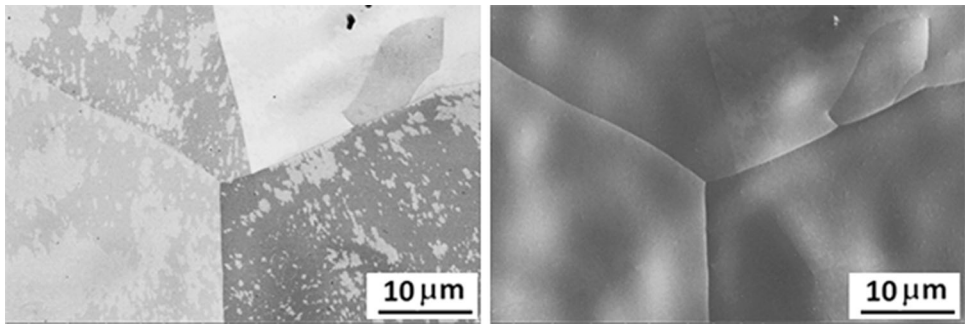

Fig. 11. SEM image of graphene film deposited on Cu at 850 W by a microwave plasma CVD process is shown on the left for the backscattering mode and on the right for th secondary electron mode. Darker regions in the backscattering image are from several layers of graphene.

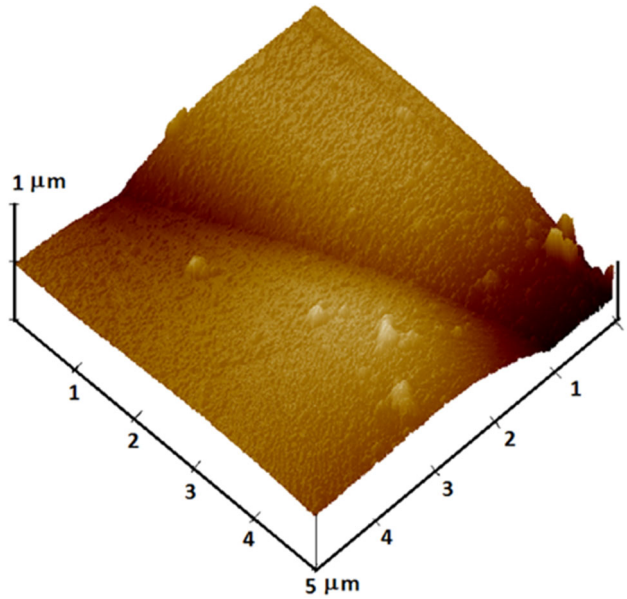

Fig. 12. AFM image in a tapping mode of the grain boundary region of the graphene film on Cu substrate grown by microwave plasma CVD at 850 W. The average roughness is found to be 35 nm. The darker regions are the valleys and brighter regions are the hills.

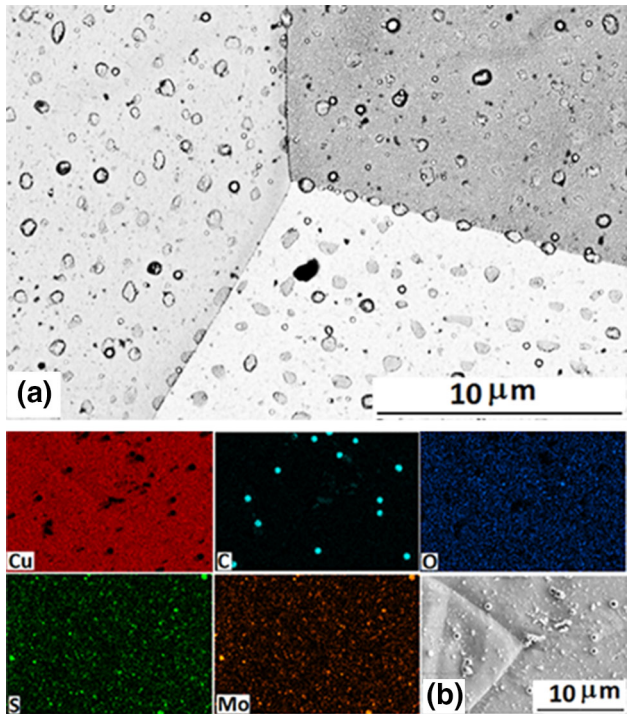

Fig. 13. (a) SEM image in secondary electron mode of MoS_2 film deposited for 1 min on graphene on Cu. (b) SEM image in secondary electron mode of MoS_2 film deposited for 45 s on graphene on Cu. The bright dots on the C signal map are the MoS_2 particulates where a C signal is absent. The irregular shaped particles are the contamination on the film surface and not part of the film.

film growth appears to depend on the orientation of Cu grains and CuO formed on the surface.

The grain boundary regions are examined in the atomic force microscope in the tapping mode and the image is shown in Fig. 12. The average roughness of the region is found to be 35 nm which is the height difference between the grain boundary valley and the adjacent grains. The Cu substrate has been etched to remove the abrasive particulates of the polishing medium. Etching is responsible for the grooves formed at the grain boundary.

SEM image of the MoS_2 film deposited for 1 min on graphene film on Cu is presented in Fig. 13a. The MoS_2 film is conformal with the graphene film and is present across the grain boundary regions and at the triple point. X-ray maps of the different elements (Cu, O, C, Mo, and S) were collected to determine the uniformity of distribution and are shown in Fig. 13b. The results illustrate that the distribution of the different elements is uniform and the O signal is weak. The signal in the O map arises from CuO present in the Cu substrate. Thus, the MoS_2 film contains a uniform distribution of Mo and S.

AFM images of MoS_2 film deposited for 1 min on all the three substrates were collected to determine the surface roughness and are shown in Fig. 14a, b, and c. The rms surface roughness of the film on sapphire, shown in Fig. 14a, is found to be 0.21 nm which is very small as a result of stable and well-

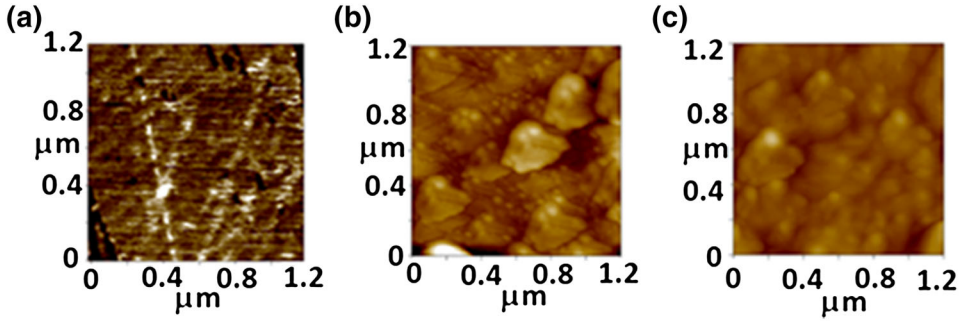

Fig. 14. (a) AFM image collected in tapping mode of MoS_2 film on sapphire, (b) Si, and (c) graphene on Cu substrate. The root mean square (RMS) surface roughness values are found to be 0.21 nm, 6.9 nm and 5.6 nm respectively in (a), (b) and (c).

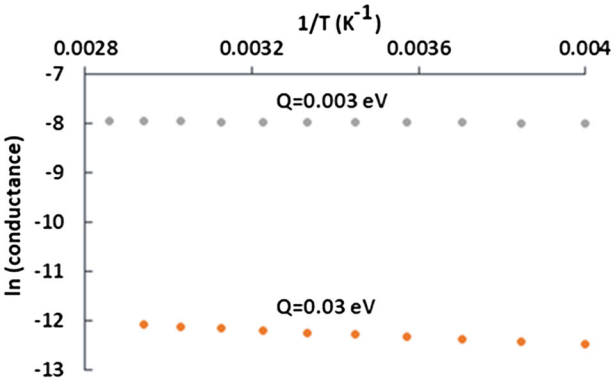

Fig. 15. ln(conductance) shown as a function of 1/T for the MoS_2 films deposited at 20 s and 1 min on sapphire substrates. The semiconducting behavior is observed for both the films. The activation energy 0.003 eV in the film deposited for 20 s and 0.03 eV in the film deposited for 1 min.

polished substrates to start with. On the other hand, the rms surface roughness of the film on Si, shown in Fig. 14b, is found to be 6.9 nm which is much higher as a result of interdiffusion and silicide formation. However, the root mean square (RMS) surface roughness of the film on graphene on Cu, shown in Fig. 14c, is found to be 5.6 nm which is a result of the surface roughness of Cu substrate that was not polished very smooth. It was previously noted, from Fig. 12, that the grain boundary regions in graphene film on Cu showed a surface roughness of 35 nm. The AFM image shown in Fig. 14c was away from the grain boundary region so that the surface roughness was smaller.

Electrical Conductance

MoS_2 films deposited on sapphire substrate have been used to measure the electrical conductance as a function of temperature. Films deposited on Si have not been used as the substrate is semiconducting. Films on graphene on Cu also could not be used for the same reason that graphene on Cu is conducting. Four probe measurements were made with the outer two probes used to input a constant current and the two inner probes used to measure the voltage drop. The magnitude of current was 1 μamp so that joule heating was negligible. A reverse current approach was used to eliminate any thermal electromotive force (EMF) at the contacts. The films deposited for 1 min and 20 s showed semiconducting behavior, however, with a very small slope as shown in Fig. 15. The activation energy, Q, was also found to be very low compared to the bandgap of MoS_2. The smaller activation energy could arise from free Mo in the film and S deficiency. S-deficient MoS_2 is known to be a degenerate *n*-type semiconductor that arises from the low-lying conduction band minimum and valence band maximum.[41] It has also been shown that doping with Nb also leads to degenerate *p*-type conduction.[41] In addition, the MoO_3 phase on the surface is also found to be effective in *p*-type doping.[42,43] However, because MoO_3 is formed at the interface between the sapphire substrate and MoS_2 film, it is concluded that *n*-type conductivity from deficiency in S is responsible for the low activation energy observed in the present films. Thus, large-area deposition with improved stoichiometry can be achieved by use of a target with excess S and lower laser fluence.[44]

CONCLUSIONS

MoS_2 films deposited on sapphire substrate showed epitaxial growth with a (0002) orientation but with S deficiency and formation of MoO_3 and Mo_4O_{11} phases. Thus, oxide substrates are responsible for MoO_3 in MoS_2. The tendency for Mo to react with O from the sapphire substrate is responsible for formation of MoO_3 at the interface. MoS_2 film was identified on the top from Raman spectroscopy and XPS. The thickness of the film was controlled by the deposition time. Excess Mo and deficiency in S are thought to be responsible for the low activation energy associated with the electrical conductance. MoS_2 films deposited on Si also showed epitaxial growth with a (0002) orientation with excess Mo; however, oxide phases were absent. The sticking coefficient of MoS_2 film on Si is lower, requiring deposition for at least 45 s for a

continuous film to form. Formation of $MoSi_2$ is found from XPS. Thus, $MoSi_2$ forms at the interface as a result of interaction of Mo with Si. MoS_2 film was not formed on Cu substrate even after 15 min of deposition as a result of reaction between Cu and MoS_2. MoS_2 films deposited on graphene film on Cu showed favorable growth with an absence of MoO_3 and Mo_4O_{11}. MoS_2 film on graphene showed characteristic Raman peaks; however, the peaks associated with graphene are suppressed by a large fluorescence background. Interaction of graphene with MoS_2 is not evident in the results from XPS. EDS spectra and x-ray maps from films deposited on sapphire, Si and graphene on Cu showed uniform distribution of Mo and S and low oxygen impurity. Uniform coverage of the film is achieved on the substrates including grain boundary regions and triple points on graphene on Cu. Thus, large area growth of MoS_2, up to 2 cm^2, on all the substrates by LPVD is favorable, provided the target density is improved and the laser pulse energy is reduced to avoid particulates in the laser-generated plume. Also, excess S in the target will help compensate for S deficiency in the film.

ACKNOWLEDGEMENTS

This work was performed in part at the Analytical Instrumentation Facility (AIF), which is supported by the State of North Carolina and the National Science Foundation (award Number ECCS-1542015). The AIF is a member of the North Carolina Research Triangle Nanotechnology Network (RTNN), a site in the National Nanotechnology Coordinated Infrastructure (NNCI). The authors wish to thank Fred Stevie with the AIF for the help in interpretation of the XPS data.

REFERENCES

1. H. Wang, L. Yu, Y.-H. Lee, Y. Shi, A. Hsu, M.L. Chin, L.-J. Li, M. Dubey, J. Kong, and T. Palacios, *Nano Lett.* 12, 4674 (2012).
2. M.-L. Tsai, S.-H. Su, J.-K. Chang, D.-S. Tsai, C.-H. Chen, C.-I. Wu, L.-J. Li, L.-J. Chen, and J.-H. He, *ACS Nano* 8, 8317 (2014).
3. A. Lipatov, P. Sharma, A. Gruverman, and A. Sinitski, *ACS Nano* 9, 8089 (2015).
4. J. Xu and X. Cao, *Chem. Eng. J.* 260, 642 (2015).
5. F. Bonaccorso, L. Colombo, G. Yu, M. Stoller, V. Tozzini, A.C. Ferrari, R.S. Ruoff, and V. Pellegrini, *Science* 347, 1246501 (2015).
6. T. Stephenson, Z. Li, B. Olsen, and D. Mitlin, *Energy Environ. Sci.* 7, 209 (2014).
7. I.L. Singer, R.N. Bolster, J. Wegand, S. Fayeulle, and B.C. Stupp, *Appl. Phys. Lett.* 57, 995 (1990).
8. K.F. Mak, C. Lee, J. Hone, J. Shan, and T.F. Heinz, *Phys. Rev. Lett.* 105, 136805 (2010).
9. K.K. Kam and B.A. Parkinson, *J. Phys. Chem.* 86, 463 (1982).
10. B. Radisavljevic, A. Radenovic, J. Brivio, V. Giacometti, and A. Kis, *Nat. Nanotechnol.* 6, 147 (2011).
11. K.S. Novoselov, D. Jiang, F. Schedin, T.J. Booth, V.V. Khotkevich, M.A. Morozov, and A.K. Gein, *Proc. Natl. Acad. Sci. USA* 102, 10451 (2005).
12. O.L. Sanchez, D. Lembke, M. Kayci, A. Radenovic, and A. Kis, *Nat. Nanotechnol.* 8, 497 (2013).
13. W. Zhu, T. Low, Y.-H. Lee, H. Wang, D.B. Farmer, J. Kong, F. Xia, and P. Avouris, *Nat. Commun.* 5, 3087 (2014).
14. Y.-H. Lee, X.-Q. Zhang, W. Zhang, M.-T. Chang, C.-T. Lin, K.-D. Chang, Y.-C. Yu, J.T.-W. Wang, C.-S. Chang, L.-J. Li, and T.-W. Lin, *Adv. Mater.* 24, 2320 (2012).
15. Y.-T. Ho, C.-H. Ma, T.-T. Luong, L.-L. Wei, T.-C. Yen, W.-T. Hsu, W.-H. Chang, Y.-C. Chu, Y.-Y. Tu, K.P. Pande, and E.Y. Chang, *Phys. Stat. Solidi RRL* 9, 187 (2015).
16. R. Moriya, T. Yamaguchi, S. Morikawa, Y. Sata, S. Masubuchi, and T. Machida, *Appl. Phys. Lett.* 105, 083119 (2014).
17. M.-Y. Lin, C.-E. Chang, C.-H. Wang, C.-F. Su, C. Chen, S.-C. Lee, and S.-Y. Lin, *Appl. Phys. Lett.* 103, 251607 (2013).
18. R. Moriya, T. Yamaguchi, I. Inoue, S. Morikawa, Y. Sata, S. Masubuchi, and T. Machida, *Appl. Phys. Lett.* 106, 223103 (2015).
19. B. Sachs, L. Britnell, T.O. Wehling, A. Eckmann, R. Jalil, B.D. Belle, A.I. Lichtenstien, M.I. Katsnelson, and K.S. Novoselov, *Appl. Phys. Lett.* 103, 251607 (2013).
20. J. Hong, Z. Hu, M. Probert, K. Li, D. Lv, X. Yang, L. Gu, N. Mao, Q. Feng, L. Xie, J. Zhang, D. Wu, Z. Zhang, C. Jin, W. Ji, X. Zhang, J. Yuan, and Z. Zhang, *Nat. Commun.* 6, 6293 (2015).
21. H. Qiu, T. Xu, Z. Wang, W. Ren, H. Nan, Z. Ni, Q. Chen, S. Yuan, F. Miao, F. Song, G. Long, Y. Shi, L. Sun, J. Wang, and X. Wang, *Nat. Commun.* 4, 2642 (2013).
22. M. van der Zande, P.Y. Huang, D.A. Chenet, T.C. Berkelbach, Y.M. You, G.-H. Lee, T.F. Heinz, D.R. Reichman, D.A. Muller, and J.C. Hone, *Nat. Mater.* 12, 554 (2013).
23. J.J. Hu, J.S. Zabinski, J.E. Bultman, J.H. Sanders, and A.A. Voevodin, *Tribol. Lett.* 24, 127 (2006).
24. T.A.J. Loh and D.H.C. Chua, *ACS Appl. Mater. Interfaces* 6, 15966 (2014).
25. C. Lee, H. Yan, L.E. Brus, T.F. Heinz, J. Hone, and S. Ryu, *ACS Nano* 4, 2695 (2010).
26. M. Dieterle, G. Weinberg, and G. Mestl, *Phys. Chem. Chem. Phys.* 4, 812 (2002).
27. M. Dieterle and G. Mestl, *Phys. Chem. Chem. Phys.* 4, 822 (2002).
28. R. Hawaldar, P. Merino, M.R. Correia, I. Bdikin, J. Grácio, J. Méndez, J.A. Martın-Gago, and M.K. Singh, *Sci. Rep.* 2, 682 (2012).
29. Y. Hao, M.S. Bharathi, L. Wang, Y. Liu, H. Chen, S. Nie, X. Wang, H. Chou, C. Tan, B. Fallahazad, H. Ramanarayan, C.W. Magnuson, E. Tutuc, B.I. Yakobson, K.F. McCarty, Y.-W. Zhang, P. Kim, J. Hone, L. Colombo, and R.S. Ruoff, *Science* 342, 720 (2013).
30. R.M. Jacobberger and M.S. Arnold, *Chem. Mater.* 25, 871 (2013).
31. C. Ferrari and J. Robertson, *Phys. Rev. B* 64, 075414 (2001).
32. K. Jagannadham, M.L. Reed, M.J. Lance, T.R. Watkins, K. Verghese, J.E. Butler, and A. Smirnov, *Diam. Relat. Mater.* 16, 50 (2007).
33. H. Hagemam, H. Bill, W. Sadowski, E. Walker, and M. Franioisc, *Solid State Commun.* 73, 447 (1990).
34. M. Balkanski, M.A. Nusimovici, and J. Reydellet, *Solid State Commun.* 7, 815 (1969).
35. A.V. Naumkin, A. Kraut-Vass, S.W. Gaarenstroom, and C.J. Powel, NIST X-ray Photoelectron Spectroscopy Database, NIST Standard Reference Database 20, Version 4.1, 2012, https://srdata.nist.gov/XPS/.
36. S. Ross and A. Sussman, *J. Phys. Chem.* 59, 889 (1955).
37. D.R. Wheeler and W.A. Brainard, Report No. NASA-TN-D-8482, E-9059, NASA Lewis Research Center, Cleveland, OH, 01 August, 1977.
38. J.H. Seo, Y.S. Lee, M.S. Jeon, J.K. Song, D.B. Han, and S.K. Rha, *J. Ceram. Process. Res.* 10, 335 (2009).
39. C. Wan, Y.N. Regmi, and B.M. Leonard, *Angew. Chem.* 126, 6525 (2014).
40. K. Oshikawa, M. Nagai, and S. Omi, *J. Phys. Chem.* 105, 9124 (2001).

41. J. Suh, T.-E. Park, D.-Y. Lin, J. Park, H.J. Jung, Y. Chen, C. Ko, C. Jang, Y. Sun, R. Sinclair, J. Chang, S. Tongay, and J. Wu, *Nano Lett.* 14, 6976 (2014).
42. L. D'Arsie, S. Esconjauregui, R. Weatherup, Y. Guo, S. Bhardwaj, A. Centeno, A. Zurutuza, C. Cepek, and J. Robertson, *Appl. Phys. Lett.* 105, 10310 (2014).
43. Z. Chen, I. Santoso, R. Wang, L.F. Xie, H.Y. Mao, H. Huang, Y.Z. Wang, X.Y. Gao, Z.K. Chen, D. Ma, A.T.S. Wee, and W. Chen, *Appl. Phys. Lett.* 96, 213104 (2010).
44. M.I. Serna, S.H. Yoo, S. Moreno, Y. Xi, J.P. Oviedo, H. Choi, H.N. Alshareef, M.J. Kim, M.M. Jolandon, and M.A.Q. Lopez, *ACS Nano* 10, 6054 (2016).